Polyhedron 249 (2024) 116782

Contents lists available at ScienceDirect

Polyhedron

journal homepage: www.elsevier.com/locate/poly

Structures and magnetic properties of a trinuclear angular [Ni_3] and a heptanuclear wheel-like [Ni_7] complexes with a Schiff base ligand

Tufan Singha Mahapatra [a,b,*], Bilash Chandra Roy [a], Biswarup Dutta [b], Jeff Lengyel [c], Michael Shatruk [c], Debashis Ray [b,*]

[a] Department of Chemistry, Faculty of Science and Technology, ICFAI University Tripura, Agartala 799210, Tripura (W), India
[b] Department of Chemistry, Indian Institute of Technology, Kharagpur 721 302, India
[c] Department of Chemistry & Biochemistry, Florida State University, Tallahassee, FL 32306, United States

ARTICLE INFO

Keywords:
Schiff base ligand
Trinuclear nickel(II) complex
Heptanuclear nickel(II) complex
Crystal structure
Antiferromagnetic interaction

ABSTRACT

The presence of large magnetic anisotropy with nickel(II) ions facilitates the single-molecule magnet (SMM) behavior in multimetallic nickel(II) complexes. Herein syntheses under ambient conditions, characterizations, crystal structures, and experimental magnetic analyses of an angular [$Ni^{II}_3L_4$] and a wheel-like [$Ni^{II}_7L_6$] complexes of general formula [$Ni_3L_2(\mu\text{-}L)_2(\mu\text{-}OH_2)_2(CF_3CO_2)_2$] (**1**) and [$Ni_7(\mu\text{-}L)_6(\mu\text{-}OMe)_6]Cl_2{\cdot}6H_2O$ (**2**) (HL = 2-{(3-ethoxypropylimino)methyl}-6-methoxyphenol) have been reported. The angular core of trimetallic neutral complex **1** is assembled using four L^-, two bridging water molecules, and two bound trifluoroacetate anions. In contrast, the heptanuclear complex **2** features a planar wheel-like arrangement with a central Ni^{II} enclosed by a {Ni^{II}_6} hexagon bound to six MeO^- and six L^-. The isolation of these two aggregates of varying nuclearity and metal ion: ligand anion ratio indicated the importance of reaction conditions and crystallization to follow the bottom-up assembly processes. Experimental magnetic studies showed antiferromagnetic interactions between the central and terminal Ni^{II} ions in complex **1** and competing ferro- and antiferromagnetic interactions in the wheel-like complex **2**.

1. Introduction

The synthetic methods for creating multinuclear nickel(II) complexes have experienced enormous growth in recent years from their structural characterizations, proposed mode of ligand-induced aggregation, applications in solid state and solution medium, magnetic and catalytic properties [1–11,58–60] and for getting information for nickel (II) bearing biomolecules [12–24,31]. The stepwise formation of coordination aggregates under the control binding of metal ions with ligand anions is a significant subject to understanding the mode of assembly processes, the role of the reaction conditions, the effect of solvents and readiness in crystal packing. N, O donor–based Schiff bases are useful in obtaining multinuclear nickel(II) molecular spin clusters [25–30]. In some cases, single-molecule magnet (SMM) behavior was identified in the laboratory-synthesized compounds having ground high-spin states and uniaxial magnetic anisotropy [3,4,32–34]. Despite the expansion and advances in Ni(II) multinuclear complexes domain, proper apprehension of the in situ generated intermediates between the starting reactants and finally produced clusters remains challenging. Ortho-vanillin-based Schiff base ligands are well known to afford a base-dependent generation of ligand anions (L^-), which can result in several {ML} and {M_2L} species upon reacting with metal ions (M) (Fig. 1) [35,45]. These fragments can further aggregate to generate stable clusters of multinuclear complexes of varying geometries in the solution pool of various ancillary ligands such as water (H_2O), hydroxide (HO^-), methoxide (MeO^-) and carboxylate (RCO_2^-) [36–46].

Herein, we report the synthetic procedures, crystal structures, and magnetic properties of trinuclear [$Ni_3L_2(\mu\text{-}L)_2(\mu\text{-}OH_2)_2(CF_3CO_2)_2$] (**1**) and heptanuclear [$Ni_7(\mu\text{-}L)_6(\mu\text{-}OMe)_6]Cl_2{\cdot}6H_2O$ (**2**) complexes on aqua and methoxido bridges, respectively. The chosen nickel(II) salts and bases were crucial for allowing water bridges as supports in **1** and assembling six methoxido groups around one nickel(II) ion in **2**. In both cases, the ligand anions (L^-) function as capping groups depending upon the solvent and metal ion-based templates. During the two aggregation progressions, the MeO— arms on L^- were utilized as and when required to provide {Ni_2L} connections. The temperature dependence of χT (χ =

* Corresponding authors at: Department of Chemistry, Faculty of Science and Technology, ICFAI University Tripura, Agartala 799210, Tripura (W), India (T. Singha Mahapatra); Department of Chemistry, Indian Institute of Technology, Kharagpur 721 302, India (D. Ray).
E-mail addresses: tufansmp@gmail.com (T. Singha Mahapatra), dray@chem.iitkgp.ac.in (D. Ray).

https://doi.org/10.1016/j.poly.2023.116782
Received 27 September 2023; Accepted 5 December 2023
Available online 8 December 2023

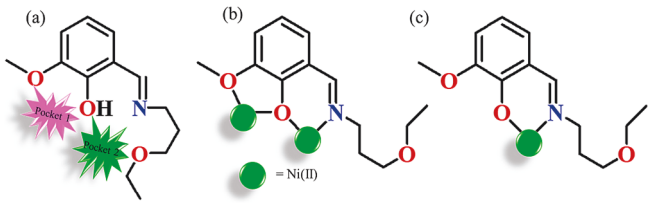

Fig. 1. (a) Chelating pockets from ligand (HL); (b and c) Two different coordination modes of the ligand in the present study.

magnetic susceptibility) was thoroughly investigated for complexes **1** and **2** to understand the magnetic exchange interactions between the Ni^{II} ions.

2. Experimental

2.1. Materials and instrumentation

Nickel(II) chloride hexahydrate, trifluoroacetic acid, lithium hydroxide monohydrate, and Nickel(II) carbonate basic hydrate [$NiCO_3{\cdot}2Ni(OH)_2{\cdot}4H_2O$] were purchased from SRL (India); 3-methoxysalicyldehyde/*ortho*-Vanillin, 3-ethoxypropylamine, and triethylamine (99 %) were purchased from Thermo Scientific Chemicals and used as received. $Ni(ClO_4)_2{\cdot}6H_2O$ and $Ni(CF_3CO_2)_2{\cdot}4H_2O$ were prepared following a procedure described in the literature [16,57]. The ligand 2-{(3-ethoxypropylimino)methyl}-6-methoxyphenol (HL) was synthesized as reported previously by our group (Scheme S1, Supplementary data) [45].

Caution!! While no such behavior was observed during the present work, perchlorate salts are potentially explosive. Therefore, they should be synthesized and used in small quantities and always handled with great care.

FTIR spectra were recorded on KBr disks (4000–400 cm^{-1}) with a Perkin-Elmer 883 spectrometer. The complexes' electronic spectra (800–200 nm) ($\sim 10^{-5}/10^{-3}$ M) in MeOH solutions were measured with Shimadzu UV 3100 UV–vis-NIR spectrophotometer. ^1H NMR (400 MHz) and ^{13}C NMR (100.6 MHz) spectra were obtained using Bruker ACF200 spectrometer. Powder X-ray diffraction (PXRD) patterns were collected at room temperature on a BRUKER AXS X-ray diffractometer (40 kV, 20 mA) using Cu-Kα radiation (λ = 1.5418 Å) over a 2θ range of 5–50°, with 4 s fixed-time counting.

2.2. Synthesis of $[Ni_3L_2(\mu\text{-}L)_2(\mu\text{-}OH_2)_2(CF_3CO_2)_2]$ (1)

Method A. NEt_3 (0.140 mL, 0.101 g, 1 mmol) was added dropwise to the yellow MeOH solution (15 mL) of HL (0.237 g, 1.00 mmol), stirring at room temperature in the air. Next to the reaction mixture, MeOH solution (10 mL) of $Ni(CF_3CO_2)_2{\cdot}4H_2O$ (0.261 g, 0.75 mmol) was mixed to yield a clear green solution. Green block-shaped crystals of **1** suitable for X-ray diffraction were grown by slow solvent evaporation of the filtered reaction mixture in the air at room temperature after 9 days.

Method B. To a yellow MeOH solution (15 mL) of HL (0.237 g, 1.00 mmol), solid $Ni(ClO_4)_2{\cdot}6H_2O$ (0.165 g, 0.75 mmol) was added under stirring conditions. Next, NEt_3 (0.140 mL, 0.101 g, 1 mmol) and solid CF_3CO_2Na (0.205 g, 1.5 mmol) were added slowly at room temperature, changing the solution color to dark green. The solution is filtered and kept for room temperature slow evaporation to obtain dark green block-shaped crystals of **1** after 8 days.

In Method A and Method B, the obtained yields for complex **1** were 62 % and 59 %, respectively.

Anal. Calcd. for $C_{56}H_{76}Ni_3N_4O_{18}F_6$ (1383.28 g mol^{-1}): C, 48.62; H, 5.54; N, 4.05. Found: C, 48.69; H, 5.58; N, 4.15. Selected FTIR bands: (KBr, cm^{-1}, vs = very strong, br = broad, s = strong, m = medium, and w = weak) 3420 (br), 1671 (s), 1624 (vs), 1471(s), 1314(m), 1244 (s), 1220 (s), 1141 (s), 1114 (s). Molar conductance, Λ_M (MeOH solution): 6 Ω^{-1} cm^2 mol^{-1}. UV–vis spectra [λ_{max}, nm (ε, L mol^{-1} cm^{-1})] (MeOH solution): 639 (29), 375 (11800), 271 (30000).

2.3. Synthesis of $[Ni_7(\mu\text{-}L)_6(\mu_3\text{-}OMe)_6]Cl_2{\cdot}6H_2O$ (2)

Solid $LiOH{\cdot}H_2O$ (0.084 g, 2 mmol) was added to the yellow MeOH solution (20 mL) of HL (0.237 g, 1.00 mmol) with stirring at room temperature. Afterwards, a methanolic solution of $NiCl_2{\cdot}6H_2O$ (0.253 g, 1.5 mmol) was treated to the yellow solid separated reaction mixture, and stirring was continued for 2 h at room temperature to afford a dark green solution. Minor insoluble impurities from the reaction mixture were separated by filtration and room temperature solvent evaporation of the clear filtrate, which provided dark brown single crystals of **2** after 4 days.

Yield: 0.745 g, 34 %. Anal. Calcd. for $C_{84}H_{138}Ni_7N_6O_{30}Cl_2$ (2193.78 g mol^{-1}): C, 45.25; H, 6.42; N, 3.77. Found: C, 45.62; H, 6.55; N, 4.12. Selected FTIR bands: (KBr, cm^{-1}, vs = very strong, br = broad, s = strong, m = medium, and w = weak) 3422 (br), 1625 (vs), 1474 (vs), 1418 (m), 1314 (m), 1225 (s), 1096 (m), 1045 (m). Molar conductance, Λ_M (MeOH solution): 161 Ω^{-1} cm^2 mol^{-1}. UV–vis spectra [λ_{max}, nm (ε, L mol^{-1} cm^{-1})] (MeOH solution): 677 (45), 361 (24100), 270 (49300).

2.4. Crystallographic data collection and refinement

Suitable single crystals of **1** and **2** were mounted on glass fiber, and the X-ray diffraction data were collected using graphite monochromated Mo-Kα radiation (λ = 0.71073 Å) on a Bruker SMART APEX-II CCD diffractometer at 298 K. For data reduction, data collection, and space group determination, the software packages utilized were SMART, SAINT-plus, and XPREP, respectively [47]. Direct methods in SHELXS-97 solved the structures [48] and subsequent Fourier analyses and then refined with full-matrix least-squares on F^2 using the SHELXL-97 [49] program package incorporated into WinGX version 1.80.05 [50]. Absorption corrections based on multi-scans were applied using the SADABS software [51]. All atoms except hydrogen were refined anisotropically. Hydrogen atoms were introduced in calculated positions and refined using fixed geometry and riding thermal parameters based on their carrier atoms. Crystallographic plots were drawn using the graphical programs DIAMOND [52] and ORTEP-III [50].

Table 1 summarizes X-ray data collection and refinement details. Crystallographic data (excluding structure factors) have been deposited with the Cambridge Crystallographic Data Centre as supplementary publications with CCDC numbers 1,480,637 and 1480638.

2.5. Magnetic measurements

Magnetic measurements were carried out on the polycrystalline samples with a Magnetic Property Measurements System MPMS-XL (Quantum Design) equipped with a superconducting quantum interference device (SQUID). The temperature dependence of magnetic susceptibility was measured in the range of 1.8–300 K in an applied field of 5000 Oe for sample **1** and 1000 Oe for sample **2**. Field-dependent magnetization measurements were conducted at 1.8 K with the magnetic field varying from 0 to 70 kOe.

3. Results and discussion

3.1. Synthetic considerations

The standard condensation reaction of 3-methoxysalicyldehyde and 3-ethoxypropylamine in 1:1 molar ratio provided the Schiff base ligand HL following a previously known procedure reported by us (Scheme S1, Supplementary data) [45]. The coordination reactivity of HL with nickel (II) ions has been explored as summarized in Fig. 2. Trinuclear species **1** was obtained *via* from the reactions of HL, NEt_3, and $Ni(CF_3CO_2)_2{\cdot}4H_2O$ in MeOH medium in 1:1:0.75 molar ratio as a green solid in 64 % yield

Table 1
Crystal parameters and refinement data of complexes **1**–**2.**

Compound reference	**Complex 1**	**Complex 2**
Chemical formula	$C_{56}H_{76}F_6N_4Ni_3O_{18}$	$C_{84}H_{126}Cl_2N_6Ni_7O_{30}$
Formula Mass	1383.28	2181.64
Crystal system	Triclinic	Cubic
Space group	$P\,\bar{1}$	$Pa\,\bar{3}$
Crystal color	Pale green	Pale green
Crystal size/mm^3	0.35 × 0.27 × 0.21	0.35 × 0.29 × 0.25
a/Å	11.959(4)	20.8122(13)
b/Å	12.820(4)	20.8122(13)
c/Å	23.041(8)	20.8122(13)
α/°	75.561(9)	90.00
β/°	79.243(9)	90.00
γ/°	64.251(8)	90.00
V/Å^3	3068.7(18)	9014.8(17)
Z	2	4
D_c/g cm^{-3}	1.497	1.608
μ (mm^{-1})	1.002	1.574
F(000)	1444	4568
T/K	293(2)	293(2)
Total reflns	35,743	102,536
R(int)	0.0567	0.1227
Unique reflns	10,743	2644
Observed reflns (I > 2σ(I))	8362	2081
Parameters	834	216
R_1 (I > 2σ(I))	0.0530, 0.1424	0.0565, 0.1673
wR_2(all reflns)		
GOF (F^2)	0.956	1.052
Largest diff peak and hole (e Å^{-3})	1.330, −0.647	0.629, −0.771
CCDC number	1,480,638	1,480,637

$R_1 = \Sigma(||F_o|-|F_c||)/\Sigma|F_o|$. $wR_2 = [\ \Sigma w(|F_o|-|F_c|)^2/\Sigma w(F_o)^2]^{1/2}$. $w = 0.75/(\sigma^2(F_o) + 0.0010F_o^2)$.

(eq 1). Variation in reactants resulted in **1** in comparable yield (68 %) from the reaction of HL, NEt_3, CF_3CO_2Na, and $Ni(ClO_4)_2{\cdot}6H_2O$ in a 1:1:1.5:0.75 molar ratio (eq 2).

$$4HL + 4NEt_3 + 3Ni(CF_3CO_2)_2{\cdot}4H_2O \rightarrow$$

$$[Ni_3L_2(\mu\text{-}L)_2(\mu\text{-}OH_2)_2(CF_3CO_2)_2] + 4(HNEt_3)(CF_3CO_2) + 10H_2O \quad (1)$$

$$4HL + 4NEt_3 + 3Ni(ClO_4)_2{\cdot}6H_2O + 6CF_3CO_2Na \rightarrow$$

$$[Ni_3L_2(\mu\text{-}L)_2(\mu\text{-}OH_2)_2(CF_3CO_2)_2] + 6NaClO_4 + 4(HNEt_3)(CF_3CO_2) + 16H_2O \quad (2)$$

Use of $LiOH{\cdot}H_2O$ and $NiCl_2{\cdot}6H_2O$ instead of NEt_3, and $Ni(CF_3CO_2)_2{\cdot}4H_2O$ in MeOH afforded green crystals of **2** in 64 % yield (eq 3).

$$6HL + 12LiOH{\cdot}H_2O + 7NiCl_2{\cdot}6H_2O + 6MeOH \rightarrow$$

$$[Ni_7(\mu\text{-}L)_6(\mu_3\text{-}OMe)_6]Cl_2{\cdot}6H_2O + 12LiCl + 48H_2O \quad (3)$$

The complexes **1** and **2** were initially characterized by FTIR and electronic spectra. Single-crystal X-ray structure analysis determined the molecular formula of $[Ni_3L_2(\mu\text{-}L)_2(\mu\text{-}OH_2)_2(CF_3CO_2)_2]$ (**1**) and $[Ni_7(\mu\text{-}L)_6(\mu_3\text{-}OMe)_6]Cl_2{\cdot}6H_2O$ (**2**). Further, the elemental compositions were confirmed by the elemental analysis as $C_{56}H_{76}F_6N_4Ni_3O_{18}$ and $C_{84}H_{126}Cl_2N_6Ni_7O_{30}$ for **1** and **2**, respectively.

The PXRD patterns of **1** and **2** match those of simulated ones from single-crystal X-ray diffraction data, confirming the phase purity of synthesized complexes in different batches. (Fig. 3).

3.2. *Description of crystal structures*

$[Ni_3L_2(\mu\text{-}L)_2(\mu\text{-}OH_2)_2(CF_3CO_2)_2]$ (1). The molecular structure of **1** bearing a discrete triangular neutral unit consisted of three Ni(II) sites, four deprotonated Schiff bases L^-, two bridging OH_2 molecules, and two coordinated trifluoroacetate anions (Fig. 4). The complex crystallized in triclinic $P\,\bar{1}$ space group with $Z = 2$ and the selected metric parameters are summarized in Table S1 in the Supplementary data. The terminal Ni (II) ions existed in a hexacoordinated NO_5 environment, whereas the central one prevailed in a hexacoordinated $\{N_2O_4\}$ environment. Terminal Ni1 and Ni3 centers basal planes comprised one imine nitrogen (N), one oxygen (O) donor atom from one L^-, one bridging phenolate O atom from another L^- and an O atom from coordinated trifluoroacetate ions. The *apical* positions of two terminal Ni(II) centers (Ni1 and Ni3) were occupied by one O donor from ligand −OMe and another from bridging water molecules on each metal ion site. As a result, the *basal* planes for these two Ni(II) centers were drawn incorporating one imine N (N1 and N4), two phenolate O (O1, O5 and O8, O12) and one acetate O (O15 and O17) donors. On the other hand, around the central Ni2, the drawn *basal* planes in Fig. 5a were instituted by two imine N (N2 and N3), two phenolate O (O1 and O8) and two water O (O4 and O11)

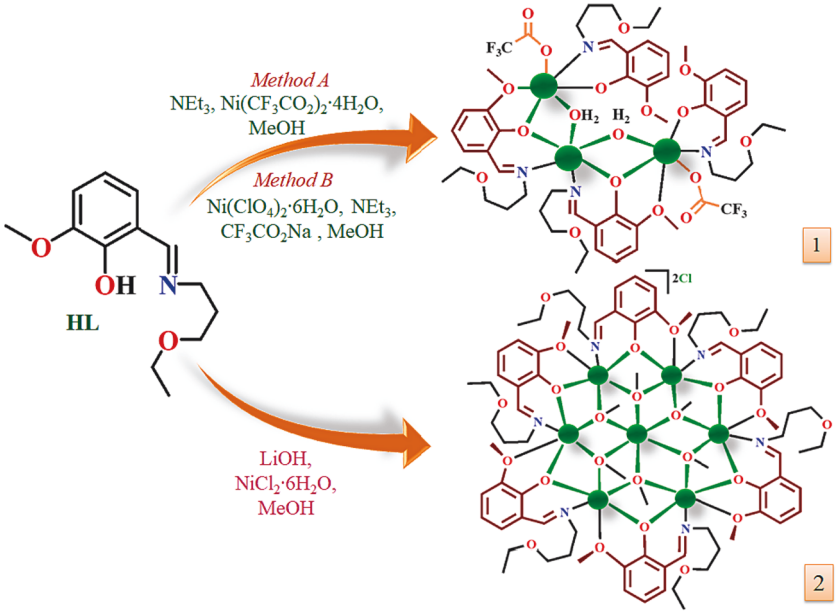

Fig. 2. Distinct synthetic paths for the construction of complexes **1** and **2.**

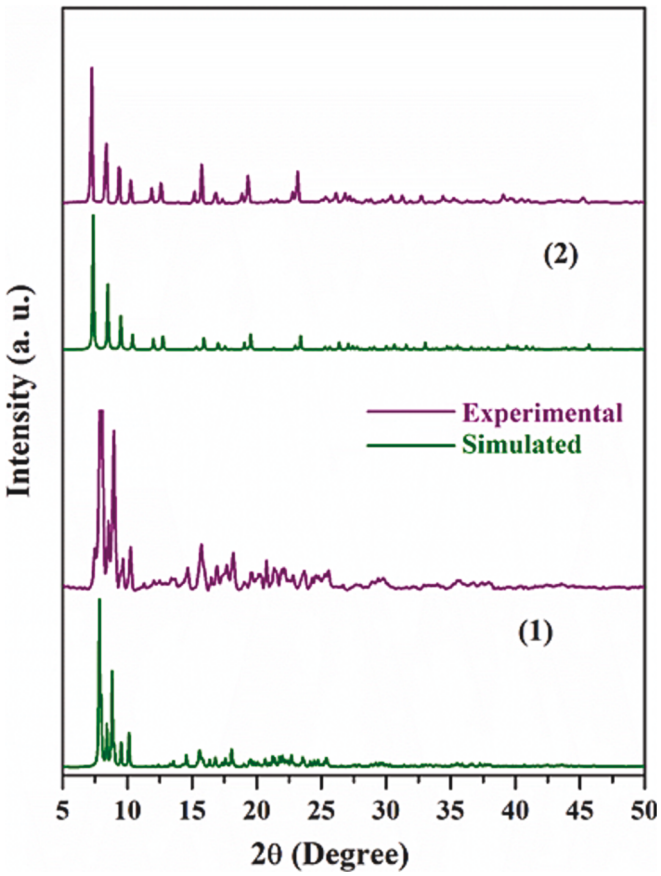

Fig. 3. Experimental (purple) and simulated (olive) PXRD patterns of **1** and **2**. ((Colour online.))

donors.

Two bridging water molecules supported the trinuclear entity and resulted in two short (2.082(3) and 2.088(3) Å) and two long (2.197(3) and 2.200(3) Å) Ni−O bonds. Where the shorter bonds are *trans* to the Ni−O bonds originating from the –OMe donors and the longer bonds are *trans* to the imine N donors (N2 and N3), making the middle Ni(II) centre in distorted O_h geometry having two elongated *cis*-Ni−O bonds. The O donors from the −OMe parts of two bridging ligand anions (μ-L^-) also provided longer Ni−O bonds of lengths 2.160(3) and 2.175(3) Å. Distorted octahedral geometry around each Ni(II) center of the angular aggregate was apparent from the wide ranges in *cis* (74.98(11) − 109.74 (12)°) and *trans* (153.31(11) − 177.53(12)°) angles at the three metal ion centers. The Ni−O_{ph}−Ni angles from O1 and O8 were found to be 104.88(13) and 104.69(12)° (Fig. 5a). The Ni−O bonds from the two bridging phenolate donors of μ-L^- span the 1.977(3)-2.054(3) Å width. The Ni•••Ni separations from the central Ni(II) (Ni2) center in complex **1** were 3.20 and 3.19 Å for Ni1•••Ni2 and Ni2•••Ni3, respectively, and the Ni1•••Ni2•••Ni3 angle was found to be of 101.35° (Fig. 5b), clearly demonstrating the angular disposition of the three Ni(II) centers involved in the aggregate.

The hydrogen atoms on O4 and O11 of both bridged water molecules were involved in strong intramolecular hydrogen bond interactions (O—H•••O, 1.821 and 1.794 Å) with the O donors (O16 and O18) of trifluoroacetate anions, respectively, which were not engaged in metal ion coordination (Fig. S1, Supplementary data).

$[Ni_7(\mu\text{-}L)_6(\mu_3\text{-}OMe)_6]Cl_2{\cdot}6H_2O$ (2). The molecular structure of **2** featured a *hexa*-methoxido-bridged flat wheel-like cationic coordination aggregate $[Ni_7(\mu\text{-}L)_6(\mu_3\text{-}OMe)_6]^{2+}$ and two charge balancing chlorides as counter anions as displayed in Fig. 6. The complex crystallized in cubic *Pa* $\bar{3}$ space group with a *Z* value of 4 and the relevant metric parameters were summarized in Table S2. In complex **2**, six L^- units coordinated to six peripheral Ni(II) ions with μ-κ^1:κ^2:κ^1 mode, which was then connected to the central Ni(II) ion through six μ_3-bridged MeO^- groups (Fig. 6). The [Ni_7] wheel core of **2** assembled as a centered hexagon around a central Ni(II) ion surrounded by a [$Ni(II)_6$] hexagon (Fig. 7). The [Ni_7] core has Ni•••Ni separations ranging from 3.124 to 3.150 Å with a wheel diameter of 6.248 Å and there are three different Ni•••Ni•••Ni angels of 59.72°, 117.85° and 180° are observed (Fig. 7). The central Ni2 atom prevailed in an octahedral {O_6} environment, whereas peripheral Ni atoms existed in the {O_5N} environment. The O−Ni2−O *cis*-angles spanned a smaller range (82.14(11)−97.86(11)°) compared to the O−Ni1−O angles (74.64(12)−109.99(13)°), whereas the *trans*-angles stretched in a 153.43(12)−165.58(7)° range.

The Ni−O_{Ph}−Ni bridge angle was 104.76(14)° with Ni−O distances in the range of 1.976(3)−2.120(3)Å, whereas the Ni−O_{Me}−Ni bridge angles spanned a narrower range within 96.24(13)−98.66(13)° with the Ni−O(Me) bonds from ligand backbone were longer (2.272(3) Å).

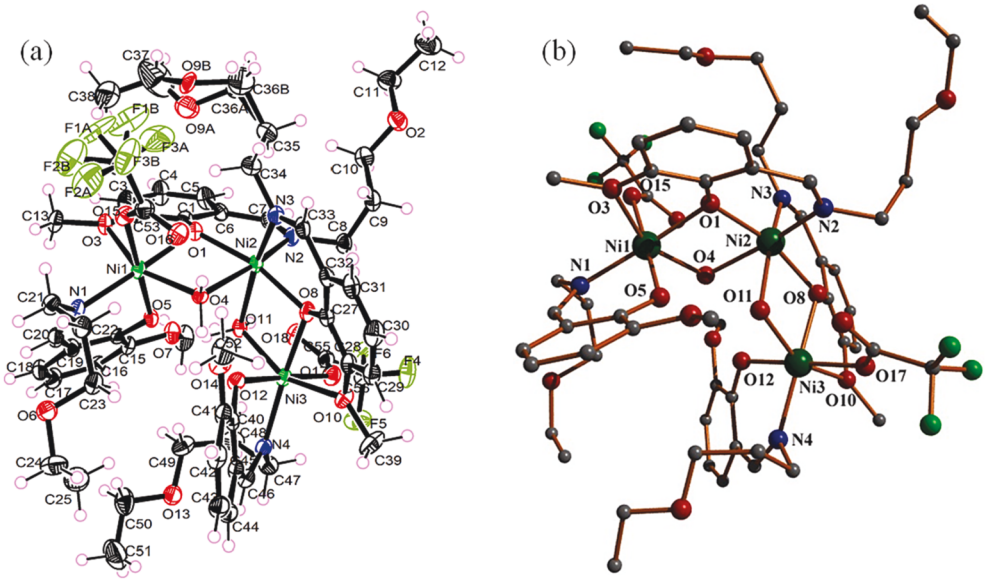

Fig. 4. (a) ORTEP view of complex **1** (50% ellipsoid probability). (b) Molecular structure of **1** (using DIAMOND), where H atoms have been excluded for the sake of clarity.

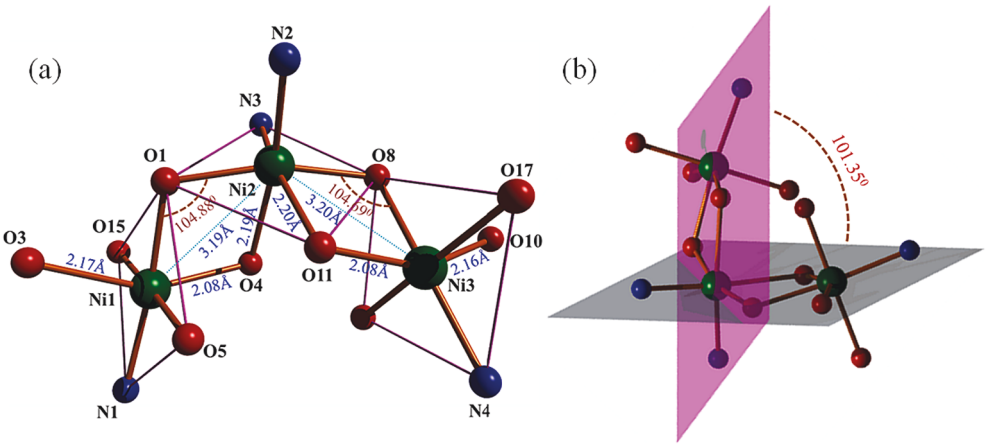

Fig. 5. (a) Core representation showing the bond lengths and angles; Color scheme: Ni, green; O, red; N, blue; C, grey. (b) Demonstration of the angular disposition of the three Ni(II) centers involved in the aggregate. ((Colour online.))

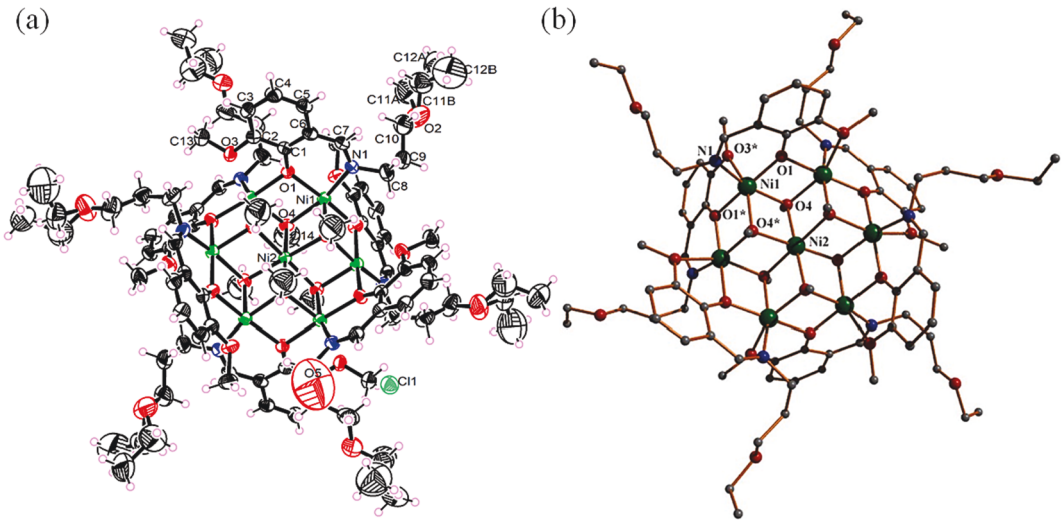

Fig. 6. (a) ORTEP representation of complex **2** (50% ellipsoid probability), (b) Molecular structure of complex **2** (using DIAMOND), with omitted H atoms for clarity.

The $[Ni_7L_6(OMe)_6]^{2+}$ cation existed as an isolated unit within the crystal lattice of **2**, with no interaction with the six lattice water molecules and two chloride counter anions (Fig. S2, Supplementary data). However, the lattice water molecules are hydrogen bonded to each other (O•••O, 2.015 Å) and chloride ions (O•••Cl, 3.131 Å) as well to construct a $[(H_2O)_6Cl_2]$ H-bonded cluster (Fig. S2, Supplementary data).

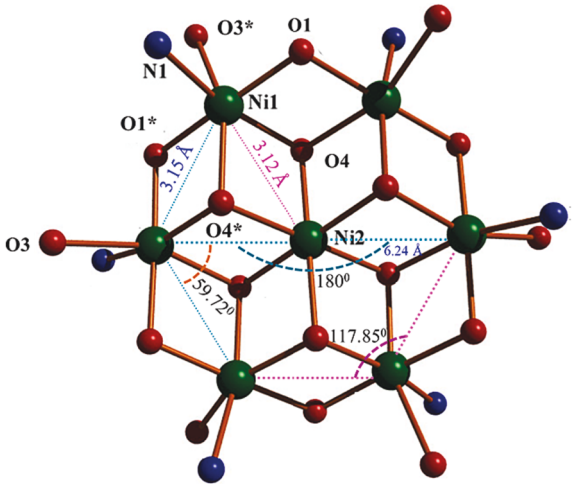

Fig. 7. Depiction of the core of the $[Ni_7]$ wheel with Ni•••Ni•••Ni bond angles and Ni•••Ni distances. Color scheme: Ni, green; O, red; N, blue; C, grey. ((Colour online.))

3.3. FTIR and electronic spectra

Complexes **1** and **2** were detected to have imine (-C═N) groups stretching frequencies at 1624 and 1625 cm^{-1}, respectively (Fig. S3, Supplementary data). Complex **1** exhibited a broad medium peak at 3422 cm^{-1}, a characteristic of aqua bridges $\bar{\nu}_{OH}$ stretching frequency. Interstitial water molecules in **2** displayed broad and medium intensity bands at 3420 cm^{-1}. The monodentate coordination ($\Delta\bar{\nu} > 300$ cm^{-1}) of trifluoroacetate groups for complex **1** was suggested by the recognition of the strong asymmetric $\bar{\nu}_{as(COO)}$ vibration and the symmetric $\bar{\nu}_{s(COO)}$ vibration at 1671 and 1314 cm^{-1}, respectively, with $\Delta\bar{\nu}$ values of 357 cm^{-1} [45].

The UV–Vis spectra of the HL, complex **1** and complex **2** were recorded in MeOH solutions ranging from 200 to 800 nm (Fig. S4, Supplementary data). At higher concentrations (~10^{-3} mol/L), complexes **1** and **2** displayed broad absorption bands at 639 nm (ε = 29 L mol^{-1} cm^{-1}) and 677 nm (ε = 45 L mol^{-1} cm^{-1}), respectively, owing to spin-allowed $^3A_{2g}(F) \rightarrow {}^3T_{1g}(F)$ transition of Ni(II) ion in slightly distorted octahedral coordination geometry [16]. Complexes **1** and **2** at lower concentrations (~10^{-5} mol/L) displayed bands at 375 nm (ε =

11800 L mol^{-1} cm^{-1}) and 361 nm (ε = 24100 L mol^{-1} cm^{-1}), respectively, which can be attributed to the ligand-to-metal charge transfer transitions [PhO$^-$ → Ni(II)] [16,25,35]. Further higher energy transitions at 226 nm (ε = 76523 L mol^{-1} cm^{-1}) and 271 nm (ε = 30000 L mol^{-1} cm^{-1}) for complex **1** and 232 nm (ε = 121033 L mol^{-1} cm^{-1}) and 270 nm (ε = 49300 L mol^{-1} cm^{-1}) for complex **2** were attributed to the mixture of n → π* and π → π* transitions related to the imine groups and benzene rings of the metal-bound ligand absorptions (Fig. 8) [16,25,35].

3.4. Magnetic properties

The temperature dependence of magnetic susceptibility (χ) was measured on polycrystalline samples of **1** and **2** under an applied field of 5000 Oe and 1000 Oe, respectively. For complex **1**, the value of χT at 300 K is 3.62 emu·K·mol^{-1}, which is slightly higher than the spin-only value of 3.00 emu·K·mol^{-1} expected for three non-interacting $S = 1$ ions. The χT gradually decreases to a minimum of 0.53 emu·K·mol^{-1} at 1.8 K (Fig. 9a). The linear part of the $1/\chi$ vs. T dependence (Fig. 9b), observed above 25 K, was fit to the Curie-Weiss law, $1/\chi = (T - \theta)/C$, resulting in a Curie constant $C = 3.89(5)$ K, which yields $g = 2.18$ for each Ni^{II} ion. The Weiss constant $\theta = -24(2)$ K indicates antiferromagnetic (AFM) interactions between the Ni^{II} ions. Field-dependent magnetization recorded at 1.8 K (Fig. 9a, inset) does not exhibit saturation, reaching the maximum value of 1.9 μ_B at the applied magnetic field $B = 70$ kOe.

The temperature dependence of χT was modeled with the PHI software [53], using to the following magnetic Hamiltonian:

$$\hat{H} = g\mu_B B\sum_{i=1}^{3}\hat{S}_i + J(\hat{S}_1 \bullet \hat{S}_2 + \hat{S}_1 \bullet \hat{S}_3) + D_{Ni}\sum_{i=1}^{3}\left(\hat{S}_z^2\right)_i \quad (4)$$

To avoid over-parametrization, the g-factor was fixed to the value of 2.18 found from the Curie-Weiss fit. The magnetic exchange between the central Ni^{II} ion (S_1) and the two terminal Ni^{II} ions (S_2 and S_3) is described by the exchange constant J, while the exchange between the terminal Ni^{II} ions is considered to be negligible, given the large distance between these metal centers. The single-ion axial zero-field splitting (ZFS) parameter, D_{Ni}, was assumed to be equal for all three Ni^{II} ions. The slightly positive slope of the χT vs. T dependence at higher temperatures also necessitated inclusion of temperature-independent paramagnetic correction (χ_{TIP}) as implemented in PHI. The best fit to the experimental data (shown with the red solid line in Fig. 9a) was obtained with $J = -5.15(2)$ cm^{-1} (AFM), $D_{Ni} = -6.9(2)$ cm^{-1}, and $\chi_{TIP} = 7.12(6) \times 10^{-4}$ emu/mol ($R^2 = 0.9994$). Meyer *et al.* [54] established that AFM interactions are observed in oxo-bridged Ni^{II} dimers when the Ni-O-Ni angle exceeds 99°, while FM interactions are observed at smaller angles. In complex **1**, the average Ni−O−Ni angles in each pair of the oxo-bridged Ni^{II} ions are 100.76° and 100.54°, thus justifying the observed moderate AFM interactions between these ions.

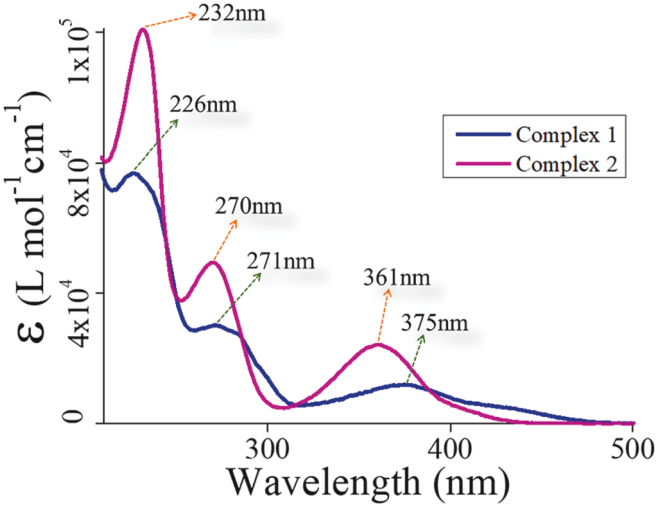

Fig. 8. Electronic spectra of the complexes **1** and **2** in MeOH.

For complex **2**, the value of χT at 300 K is 5.56 emu·K·mol^{-1}, which is substantially lower than the spin-only value of 7.00 emu·K·mol^{-1} expected for seven non-interacting $S = 1$ ions. As the temperature is lowered, the value of χT continuously decreases, reaching a minimum value of 0.67 emu·K·mol^{-1} at 1.8 K (Fig. 10). The linear part of the $1/\chi$ vs. T dependence was fit to the Curie-Weiss law above 150 K, resulting in a Curie constant $C = 8.34(5)$ emu·K·mol^{-1}, which yields $g = 2.18$ for each Ni^{II} ion, in good agreement with the g-values reported previously for similar heptanuclear Ni^{II} complexes [55,56]. The large negative value of the Weiss constant, $\theta = -147(2)$ K, indicates strong AFM coupling between the Ni^{II} ions. The assumption of strong magnetic interactions is also in agreement with the fact that the field-dependent magnetization recorded at 1.8 K reaches the maximum of only 6.99 μ_B at the magnetic field $B = 70$ kOe, as compared to the saturation value of 14 μ_B expected for seven non-interacting $S = 1$ ions.

The temperature dependence of χT was modeled with the following magnetic Hamiltonian:

$$\hat{H} = g\mu_B B\sum_{i=1}^{7}\hat{S}_i + J_1\sum_{i=2}^{7}\hat{S}_1 \bullet \hat{S}_i + J_2\left(\sum_{i=2}^{6}\hat{S}_i \bullet \hat{S}_{i+1} + \hat{S}_2 \bullet \hat{S}_7\right) + D_{Ni}\sum_{i=1}^{7}\left(\hat{S}_z^2\right)_i \quad (5)$$

To avoid over-parametrization, the g-factor was fixed to the value of 2.18 found from the Curie-Weiss fit. The high symmetry of the complex implies that only two magnetic exchange constants should be considered: the J_1 describing the coupling between the central Ni^{II} ion (S_1) and the peripheral Ni^{II} ions (S_2 through S_7) and the J_2 describing the coupling between the peripheral Ni^{II} ions. The ZFS parameter D_{Ni} was set equal for all seven Ni^{II} ions, also to avoid over-parametrization. The best fit to the experimental data (shown with the red solid line in Fig. 10a) was obtained with $J_1 = 12.3(5)$ cm^{-1}, $J_2 = -44.1(8)$ cm^{-1}, and $D_{Ni} = -2.58(3)$ cm^{-1} ($R^2 = 0.9887$). These values imply rather strong AFM interactions between the peripheral Ni^{II} ions and moderate competing ferromagnetic (FM) interactions between these peripheral ions and the central Ni^{II} ion. It is interesting to compare the values of the magnetic exchange parameters found for complex **2** to those reported for other disc-like Ni$_7$ complexes. In the majority of cases described in the literature, the decrease in the χT value with temperature was not as pronounced as in the present case. Moreover, in some cases, dominant FM interactions were observed. The reasons for the unusually strong AFM coupling between the peripheral Ni^{II} ions in **2** can be found in the structural parameters observed for this complex, in accordance with the aforementioned criterion derived by Meyer *et al* [54]. For example, Hayami *et al.* [56] (see the code QUPFEP in the Cambridge Structural Database) observed weak FM interactions between the central and peripheral Ni^{II} ions ($J_1 = 0.31$ cm^{-1}) and substantial FM interactions between the peripheral Ni^{II} ions ($J_2 = 7.25$ cm^{-1}), which correlate with the observed ranges of the Ni−O−Ni angles, $\alpha_{inner} = 97.63$–$99.80°$ and $\alpha_{peri} = 94.53$–$99.68°$, respectively. In contrast, Gheorghe *et al.* (HOMRAF) [55] reported competing FM and AFM interactions of moderate strength, $J_1 = 5.6$ cm^{-1} (FM) and $J_2 = -4.8$ cm^{-1} (AFM), which correlate with the corresponding angles of $\alpha_{inner} = 96.06$–$97.68°$ and $\alpha_{peri} = 97.74$–$101.20°$. Similar observations were made by Hayami *et al.* [33] for another heptanuclear complex (PAZBIE) with the $J_1 = 6.9$ cm^{-1} (FM) and $J_2 = -3.4$ cm^{-1} (AFM) correlating with the angle ranges of $\alpha_{inner} = 95.00$–$95.91°$ and $\alpha_{peri} = 96.00$–$103.50°$, respectively.

In contrast to these well-analyzed cases, in complex **2** we observe increased Ni−O−Ni angles at the periphery of the complex, in the range of 98.35–104.76°, which explains the stronger AFM exchange between the peripheral Ni^{II} ions. On the other hand, The Ni−O−Ni angles

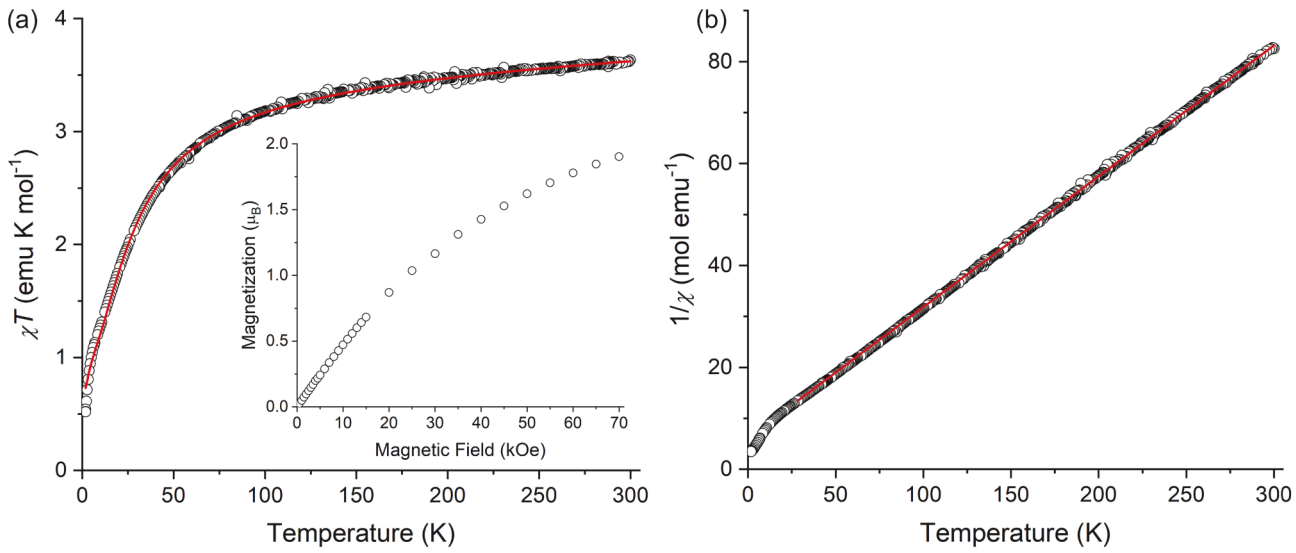

Fig. 9. Temperature dependence of χT (a) and $1/\chi$ (b) for complex **1**. The solid red lines represent theoretical fits to the Hamiltonian given in Eq. (4) and to the Curie-Weiss law, respectively. The inset in panel (a) shows field-dependent magnetization measured at 1.8 K. ((Colour online.))

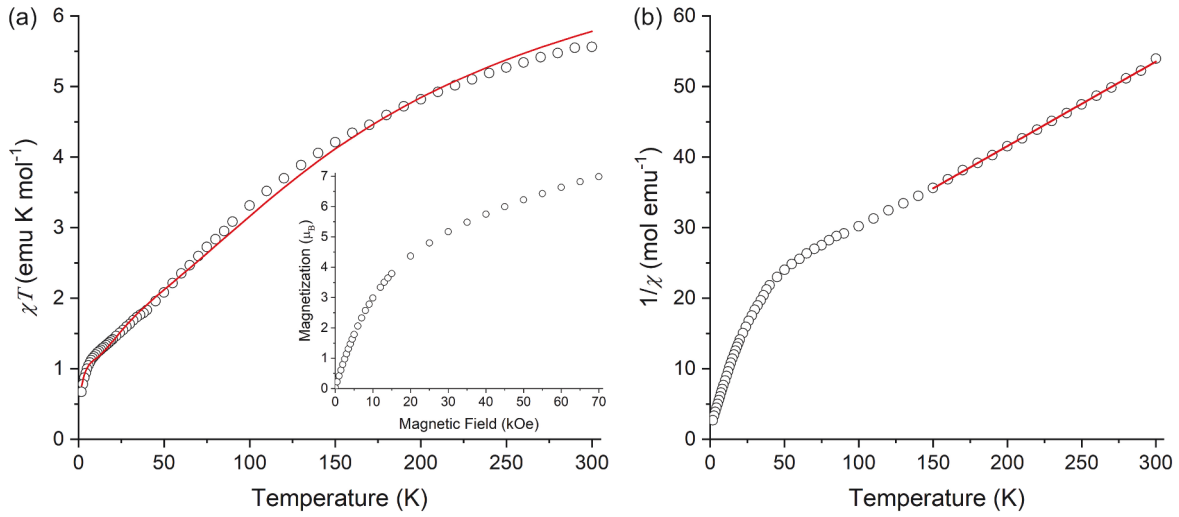

Fig. 10. Temperature dependence of χT (a) and $1/\chi$ (b) for complex **2**. The solid red lines represent theoretical fits to the Hamiltonian given in Eq. (5) and to the Curie-Weiss law, respectively. The inset in panel (a) shows field-dependent magnetization measured at 1.8 K. ((Colour online.))

between the central and peripheral Ni^{II} ions range from 96.24 to 98.66°, thus well justifying the FM exchange. The comparison of the crystal structure parameters and magnetic data provided in Table 2 clearly shows that our modeling has resulted in physically meaningful values of the exchange constants.

4. Conclusion

Control of the reaction conditions using one type of Schiff base anion resulted in two different coordination aggregates of varying arrangement of nickel(II) ions and the linkers inside the aggregates. Synthesis and properties of two new members of [Ni_3] and [Ni_7] family of multimetallic complexes have been studied. In the first type, the L-angle between Ni1···Ni2···Ni3 is 101.35°, which is appropriate for the exploitation of two aqua bridges. In contrast, in complex **2**, the Ni1···Ni1*···Ni2 angle reduces to 59.72° allowing the μ_3-methoxide bridging. Modelling the magnetic data of these complexes led to a good agreement with the previously reported trend correlating the Ni−O−Ni angle at the bridging oxide with the magnetic exchange coupling. In the angular complex [$Ni^{II}_3L_4$] (**1**), moderate-strength antiferromagnetic

Table 2
Crystal structure parameters and magnetic exchange constants for complex **2** and similar heptanuclear complexes are reported in the literature.

CSD Code	d(Ni-Ni)$_{inner}$, Å	d(Ni-Ni)$_{peri}$, Å	Ni-O-Ni (α_{inner}, deg)	Ni-O-Ni (α_{peri}, deg)	Magnetic Exchange Constants (in cm^{-1})	Reference
Complex **2**	3.124	3.150	96.24–98.66	98.35–104.76	$J_1 = 12.3$, $J_2 = -44.1$	*This work*
HOMRAF	3.077–3.096	3.081–3.095	96.06–97.68	97.74–101.20	$J_1 = 5.6$, $J_2 = -4.8$	[55]
PAZBIE	3.079	3.084	95.00–95.91	96.00–103.50	$J_1 = 6.87$, $J_2 = -3.41$	[33]
QUPFEP	3.100	3.107	97.63–99.80	99.68–94.53	$J_1 = 0.31$, $J_2 = 7.25$	[56]

interactions between the central and terminal Ni^{II} ions are observed. On the other hand, the wheel-like complex $[Ni^{II}_7L_6]$ (**2**) exhibits competing magnetic interactions, with moderate ferromagnetic coupling between the central and peripheral Ni^{II} ions and stronger antiferromagnetic coupling between the peripheral Ni^{II} ions.

CRediT authorship contribution statement

Tufan Singha Mahapatra: Conceptualization, Investigation, Methodology, Software, Writing – original draft, Writing – review & editing. **Bilash Chandra Roy:** Data curation, Methodology, Investigation. **Biswarup Dutta:** Data curation, Formal analysis, Investigation, Methodology. **Jeff Lengyel:** Data curation, Investigation, Methodology, Software. **Michael Shatruk:** Data curation, Formal analysis, Methodology, Software, Writing – original draft. **Debashis Ray:** Conceptualization, Supervision, Writing – original draft, Writing – review & editing.

Declaration of competing interest

The authors declare that they have no known competing financial interests or personal relationships that could have appeared to influence the work reported in this paper.

Data availability

Data will be made available on request.

Acknowledgements

TSM acknowledges the Department of Chemistry, ICFAI University Tripura. BCR acknowledges ICFAI University Tripura for the fellowship. We are also thankful to DST, New Delhi, for providing the Single Crystal X-ray Diffractometer facility in the Department of Chemistry, IIT Kharagpur under its FIST program. The authors acknowledge Dr. Dipmalya Basak from the National Institute of Technology Sikkim for his assistance in fixing the disorder in both crystal structures. Magnetic studies at Florida State University (FSU) were performed with the support from the U.S. National Science Foundation (award CHE-2300779). The project also used resources provided by the Materials Characterization Laboratory (FSU075000MAC) at the FSU Department of Chemistry and Biochemistry.

Appendix A. Supplementary data

Supplementary data to this article can be found online at https://doi.org/10.1016/j.poly.2023.116782.

References

[1] N.M. Bonanno, A.J. Lough, M.T. Lemaire, A trinuclear nickel(II) cluster containing a ditopic redox active ligand: Structural and magnetic properties, Polyhedron 183 (2020), 114536.
[2] C. Papatriantafyllopoulou, E. Diamantopoulou, A. Terzis, V. Tangoulis, N. Lalioti, S.P. Perlepes, High-nuclearity nickel(II) clusters: Ni13 complexes from the use of 1-hydroxybenzotriazole, Polyhedron 28 (2009) 1903–1911.
[3] S. Hameury, L. Kayser, R. Pattacini, P. Rosa, A.-L. Barra, P. Braunstein, Synthesis, Structures, and Single-Molecule Magnet Behaviour of High-Nuclearity Nickel(II) Dicubane-Type Complexes with Pyridyl-Alcohol Ligands, ChemPlusChem 80 (2015) 1312–1320.
[4] S. Hameury, L. Kayser, R. Pattacini, G. Rogez, W. Wernsdorfer, P. Braunstein, Synthesis of cubane-type Ni(ii) complexes from pyridyl-alcohol ligands; their single-molecule magnet behaviour, Dalton Trans. 42 (2013) 5013–5024.
[5] A.F. Orsino, M. Gutiérrez del Campo, M. Lutz, M.-E. Moret, Enhanced Catalytic Activity of Nickel Complexes of an Adaptive Diphosphine-Benzophenone Ligand in Alkyne Cyclotrimerization, ACS Catal. 9 (2019) 2458–2481.
[6] P. li, M. Niu, M. Hong, S. Cheng, J. Dou, Effect of structure and composition of nickel(II) complexes with salicylidene Schiff base ligands on their DNA/protein interaction and cytotoxicity, J. Inorg. Biochem., 137 (2014) 101-108.
[7] R. Luo, C.-G. Xu, J.-P. Tong, H.-Y. Shi, X.-J. Kong, Y.-H. Fan, F. Shao, Synthesis, structure, and magnetism of a novel series of trinuclear nickel(ii) clusters, CrystEngComm 24 (2022) 5987–5994.
[8] Y. Tan, Y. Lei, Synthesis and crystal structures of copper, nickel and zinc complexes derived from 2-((2-(pyrrolidin-1-yl)ethylimino)methyl)phenol with antimicrobial activity, Polyhedron 231 (2023), 116270.
[9] R. Carballo, A.B. Lago, M. Vázquez-Toirán, L. Estévez, E.M. Vázquez-López, Square-planar and octahedral nickel complexes of an acylhydrazone ligand and the serendipitous isolation of a potential octahedral nickel acylhydrazone precursor, CrystEngComm (2023).
[10] J.W. Shin, A.R. Jeong, S.Y. Lee, C. Kim, S. Hayami, K.S. Min, Trinuclear nickel and cobalt complexes containing unsymmetrical tripodal tetradentate ligands: syntheses, structural, magnetic, and catalytic properties, Dalton Trans. 45 (2016) 14089–14100.
[11] A.K. Ghosh, T. Singha Mahapatra, R. Clérac, C. Mathonière, V. Bertolasi, D. Ray, Direct C-N Coupling in an in-Situ Ligand Transformation and the Self-Assembly of a Tetrametallic [NiII4] Staircase, Inorg. Chem. 54 (2015) 5136–5138.
[12] A.M. Barrios, S.J. Lippard, Interaction of Urea with a Hydroxide-Bridged Dinuclear Nickel Center: An Alternative Model for the Mechanism of Urease, J. Am. Chem. Soc. 122 (2000) 9172–9177.
[13] B.K. Kundu, S. Pragti, A. Biswas, S. Mondal, S.M. Mazumdar, S. Mobin, Mukhopadhyay, Unveiling the urease like intrinsic catalytic activities of two dinuclear nickel complexes towards the in situ syntheses of aminocyanopyridines, Dalton Trans. 50 (2021) 4848–4858.
[14] C.-Y. Tsai, F.-Y. Cheng, K.-Y. Lu, J.-T. Wu, B.-H. Huang, W.-A. Chen, C.-C. Lin, B.-T. Ko, Dinuclear and Trinuclear Nickel Complexes as Effective Catalysts for Alternating Copolymerization on Carbon Dioxide and Cyclohexene Oxide, Inorg. Chem. 55 (2016) 7843–7851.
[15] G.E. Bekmukhamedov, A.V. Sukhov, A.M. Kuchkaev, A.M. Kuchkaev, K. R. Khayarov, A.B. Dobrynin, V.M. Babaev, D.G. Yakhvarov, Catalytic performance of nickel(II) complexes bearing 1,10-phenanthroline based ligands in homogeneous ethylene oligomerization, Polyhedron 223 (2022), 115978.
[16] T.S. Mahapatra, S. Chaudhury, S. Dasgupta, V. Bertolasi, D. Ray, Dinuclear nickel complexes of divergent Ni···Ni separation showing ancillary ligand addition and bio-macromolecular interaction, New J. Chem. 40 (2016) 2268–2279.
[17] S. Gandhimathi, M. Theetharappan, N.S.P. Bhuvanesh, M.A. Neelakantan, Crystal structure, theoretical and experimental electronic structure and DNA/BSA protein interactions of nickel(II) N2O2 tetradentate Schiff base complexes, Polyhedron 138 (2017) 88–102.
[18] E. Keshavarzian, Z. Asadi, M. Kucerakova, M. Dusek, B. Rastegari, DNA interaction and BSA binding of O-vanillin-based new Schiff base Co(III) and Ni(II) complexes: Theoretical, experimental, antibacterial and anticancer studies, Polyhedron 223 (2022), 115987.
[19] N. Selvakumaran, N.S.P. Bhuvanesh, A. Endo, R. Karvembu, Synthesis, structure, DNA and protein binding studies, and cytotoxic activity of nickel(II) complexes containing 3,3-dialkyl/aryl-1-(2,4-dichlorobenzoyl)thiourea ligands, Polyhedron 75 (2014) 95–109.
[20] A. Patra, H. Puschmann, S.C. Manna, Bidentate Schiff base coordinated square planer nickel(II) complexes: Synthesis, crystal structure, DFT/TD-DFT Calculation and DNA/protein binding, Polyhedron 201 (2021), 115146.
[21] K.N.A. Rahman, J. Haribabu, C. Balachandran, N.S.P. Bhuvanesh, R. Karvembu, A. Sreekanth, Copper, nickel and zinc complexes of 3-acetyl coumarin thiosemicarbazone: Synthesis, characterization and in vitro evaluation of cytotoxicity and DNA/protein binding properties, Polyhedron 135 (2017) 26–35.
[22] A. Paul, A. Figuerola, H. Puschmann, S.C. Manna, Double μ2-(phenoxido)-bridged dinuclear and polynuclear nickel(II) complexes: Magnetic properties and DNA/protein interaction, Polyhedron 157 (2019) 39–48.
[23] A. Barma, D. Ghosh, P. Karmakar, P. Roy, Synthesis and characterization of a mononuclear nickel(II) complex with N, O-donor ligand: Its DNA/HSA protein binding properties and tumor suppressive function, J. Mol. Struct. 1250 (2022), 131687.
[24] M. Zaki, S. Hairat, S. Kamaal, N.H. Aljarba, N.S. Al–Johani, S. Alkahtani, Synthesis, crystal structure elucidation and DNA/HSA binding profile of Ni(II) complex of Schiff base derived from 3–ethoxy salicylaldehyde and o–phenylenediamine, J. Mol. Struct., 1265 (2022) 133351.
[25] M. Pait, A. Bauzá, A. Frontera, E. Colacio, D. Ray, A New Family of Ni4 and Ni6 Aggregates from the Self-Assembly of [Ni2] Building Units: Role of Carboxylate and Carbonate Bridges, Inorg. Chem. 54 (2015) 4709–4723.
[26] P.S. Perlepe, A.A. Athanasopoulou, K.I. Alexopoulou, C.P. Raptopoulou, V. Psycharis, A. Escuer, S.P. Perlepes, T.C. Stamatatos, Structural and magnetic variations in tetranuclear NiII clusters: the effect of the reaction solvent and ligand substitution on product identity, Dalton Trans. 43 (2014) 16605–16609.
[27] L.-Q. Wei, K. Zhang, Y.-C. Feng, Y.-H. Wang, M.-H. Zeng, M. Kurmoo, Microwave versus Traditional Solvothermal Synthesis of Ni7II Discs: Effect of Ligand on Exchange Reaction in Solution Studied by Electrospray Ionization-Mass Spectroscopy and Magnetic Properties, Inorg. Chem. 50 (2011) 7274–7283.
[28] A. Panja, S. Adak, P. Brandão, Ľ. Dlháň, R. Boča, Syntheses, Structures and Magnetic Properties of Ferromagnetically/Antiferromagnetically Coupled Penta- and Hexanuclear Azido-Bridged Nickel(II) Coordination Compounds, Eur. J. Inorg. Chem. 2020 (2020) 2362–2371.
[29] L. Shen, P. Hu, X.-J. Yang, H. Xu, Y.-L. Huang, C. Redshaw, Q.-L. Zhang, Structural and magnetic characterization of tetranuclear [Ni(II)2Ln(III)2] complexes bearing tetra-branched Schiff base ligands, Polyhedron 212 (2022), 115584.
[30] S.J. Munshi, M.H. Sadhu, S. Kundu, C. Savani, S.B. Kumar, Synthesis, characterization and structures of binuclear copper(II) and polynuclear cobalt(II), nickel(II) and cadmium(II) complexes involving N4-donor pyrazolyl based ligand and dicyanamide as bridging ligand, J. Mol. Struct. 1209 (2020), 127984.
[31] R. Herchel, I. Nemec, M. Machata, Z. Trávníček, Solvent-induced structural diversity in tetranuclear Ni(ii) Schiff-base complexes: the first Ni4 single-molecule

magnet with a defective dicubane-like topology, Dalton Trans. 45 (2016) 18622–18634.
[32] S. Bera, S. Majumdar, S. Chattopadhyay, A comprehensive overview on the synthesis and characterization of nickel, copper and hetero-nuclear copper/lanthanoid and nickel/lanthanoid complexes with salicylaldehyde-based azine ligands, Polyhedron 225 (2022), 116068.
[33] F. Kobayashi, R. Ohtani, S. Teraoka, W. Kosaka, H. Miyasaka, Y. Zhang, L. F. Lindoy, S. Hayami, M. Nakamura, Syntheses, structures and magnetic properties of tetranuclear cubane-type and heptanuclear wheel-type nickel(ii) complexes with 3-methoxysalicylic acid derivatives, Dalton Trans. 46 (2017) 8555–8561.
[34] A. Scheurer, K. Gieb, M.S. Alam, F.W. Heinemann, R.W. Saalfrank, W. Kroener, K. Petukhov, M. Stocker, P. Müller, Synthesis, magnetic properties, and STM spectroscopy of an unprecedented octanuclear chloro-bridged nickel(ii) double cubane, Dalton Trans. 41 (2012) 3553–3561.
[35] B.C. Roy, B. Dutta, D. Basak, S. Debnath, D. Ray, T.S. Mahapatra, Investigations on a mononuclear Cu(II) Schiff base complex: theoretical calculations, catechol oxidase activity, and protein binding interaction analysis, New J. Chem. 47 (2023) 11928–11944.
[36] S. Shit, M. Nandy, G. Rosair, C.J. Gómez-García, J.J. Borras Almenar, S. Mitra, A ferromagnetically coupled single hydroxido bridged tetranuclear nickel(II) Schiff base complex incorporating a Ni4O4 cubane core: Crystal structure and magnetic study, Polyhedron 61 (2013) 73–79.
[37] S.S. Tandon, S.D. Bunge, N. Patel, J. Sanchiz, H-bonding directed formation of 1D-single chains, 2D-sheets, and 3D structures in magnetically coupled tetranuclear nickel(II) complexes with incomplete double cubane core, Polyhedron 123 (2017) 361–375.
[38] A.N. Gusev, I. Nemec, R. Herchel, Y.I. Baluda, M.A. Kryukova, N.N. Efimov, M. A. Kiskin, W. Linert, A new series of Schiff base Ni(II)4 cubanes: Evaluation of magnetic coupling via carboxylate bridges, Polyhedron 196 (2021), 115017.
[39] S. Liu, S. Wang, F. Cao, H. Fu, D. Li, J. Dou, Crystallization condition-controlled assembly of oxygen-bridged tetranuclear and hexanuclear Ni(ii) clusters: syntheses, structures and properties, RSC Adv. 2 (2012) 1310–1313.
[40] A.K. Ghosh, M. Shatruk, V. Bertolasi, K. Pramanik, D. Ray, Self-Assembled Tetra- and Pentanuclear Nickel(II) Aggregates From Phenoxido-Based Ligand -Bound Ni2 Fragments: Carboxylate Bridge Controlled Structures, Inorg. Chem. 52 (2013) 13894–13903.
[41] I. Nemec, R. Herchel, M. Machata, Z. Trávníček, Tetranuclear Ni(ii) and Co(ii) Schiff-base complexes with an M4O6 defective dicubane-like core: zero-field SMM behavior in the cobalt analogue, New J. Chem. 41 (2017) 11258–11267.
[42] M.E. Slater-Parry, J.P. Durrant, J.M. Howells, M.B. Pitak, P.N. Horton, W. T. Klooster, S.J. Coles, H.M. O'Connor, E.K. Brechin, A.-L. Barra, L.F. Jones, Crowding out: ligand modifications and their structure directing effects on brucite-like Mx(μ3-OH)y (M = Co(ii), Ni(ii)) core growth within polymetallic cages, Dalton Trans. 48 (2019) 1477–1488.
[43] T.S. Mahapatra, A. Bauzá, D. Dutta, S. Mishra, A. Frontera, D. Ray, Carboxylate Coordination Assisted Aggregation for Quasi-Tetrahedral and Partial-Dicubane [Cu4] Coordination Clusters, ChemistrySelect 1 (2016) 64–75.
[44] T. Singha Mahapatra, A. Roy, S. Chaudhury, S. Dasgupta, S. Lal Shrivastava, V. Bertolasi, D. Ray, Trapping of a Methanoato Bridge in μ-1,1,3,3 Mode for [Cu4] Aggregate Formation: Synthesis, Steric Control on Nuclearity, Antimicrobial Activity, and DNA-Interaction Properties, Eur. J. Inorg. Chem. 2017 (2017) 769–779.
[45] T. Singha Mahapatra, D. Basak, S. Chand, J. Lengyel, M. Shatruk, V. Bertolasi, D. Ray, Competitive coordination aggregation for V-shaped [Co3] and disc-like [Co7] complexes: synthesis, magnetic properties and catechol oxidase activity, Dalton Trans. 45 (2016) 13576–13589.
[46] R.-X. Zhao, J. Wang, D.-W. Jing, H.-J. Zhang, C. Feng, G.-Y. Li, Syntheses, crystal structure and property of a heptanuclear cluster, Inorg. Chem. Commun. 111 (2020), 107597.
[47] Saint, Smart and XPREP, Siemens Analytical X-ray Instruments Inc, Madison, WI (1995).
[48] G.M. Sheldrick, Acta Cryst. A 64 (2008) 112–122.
[49] G.M. Sheldrick, Crystal Structure Refinement with SHELXL, Acta, Crystallogr. C 71 (2015) 3–8.
[50] L.J. Farrugia, J. Appl. Crystallogr. 45 (2012) 849–854.
[51] G. M. Sheldrick, SADABS:Software for Empirical Absorption Correction; University of Göttingen, Institute fur AnorganischeChemiederUniversitat, Göttingen, Germany (1999–2003).
[52] DIAMOND, Visual Crystal Structure Information System, version 3.1; Crystal Impact: Bonn, Germany (2004).
[53] N.F. Chilton, R.P. Anderson, L.D. Turner, A. Soncini, K.S. Murray, PHI: A powerful new program for the analysis of anisotropic monomeric and exchange-coupled polynuclear d- and f-block complexes, J. Comput. Chem. 34 (2013) 1164–1175.
[54] A. Das, F.J. Klinke, S. Demeshko, S. Meyer, S. Dechert, F. Meyer, Reversible Solvatomagnetic Effect in Novel Tetranuclear Cubane-Type Ni4 Complexes and Magnetostructural Correlations for the [Ni4(μ3-O)4] Core, Inorg. Chem. 51 (2012) 8141–8149.
[55] R. Gheorghe, G. Andreea Ionita, C. Maxim, A. Caneschi, L. Sorace, M. Andruh, Aggregation of heptanuclear [MII7] (M = Co, Ni, Zn) clusters by a Schiff-base ligand derived from o-vanillin: Synthesis, crystal structures and magnetic properties, Polyhedron 171 (2019) 269–278.
[56] S. Kusumoto, Y. Kim, M. Nakamura, L.F. Lindoy, S. Hayami, Ferromagnetically Coupled Hydroxo-bridged Heptanuclear Ni(II) Wheel Cluster with S = 7 Ground Spin State, Chem. Lett. 49 (2019) 24–27.
[57] M.J. Baillie, D.H. Brown, K.C. Moss, D.W.A. Sharp, Anhydrous metal trifluoroacetates, J. Chem. Soc. A 3110–3114 (1968).
[58] S. Kamaal, M. Usman, M. Afzal, A. Alarifi, A. Ali, R. Das, P. Lama, M. Ahmad, A new copper(II)-based layered coordination polymer: Crystal structure, topology, QTAIM analysis, experimental and theoretical magnetic properties based on DFT combined with broken-symmetry formalism (BS-DFT), Polyhedron 193 (2021), 114881.
[59] S. Kamaal, M.J. Alam, M. Afzal, A. Ali, S. Ahmad, A. Alarifi, R. Das, M. Gupta, M. Ahmad, Fabrication of a new 2D Co(II)-organic framework tuned by semi-flexible dicarboxylate and 1,4-bis(4-pyridinylmethyl)piperazine ligands: Topology, DFT/UB3LYP calculations, Hirshfeld surface analysis and magnetic studies, J. Mol. Struct. 1229 (2021), 129616.
[60] S. Kamaal, M. Gupta, R. Mishra, A. Ali, A. Alarifi, M. Afzal, R. Das, M. Ahmad, A three-dimensional pentanuclear Co(II) coordination polymer: structural topology, hirshfeld surface analysis and magnetic properties, ChemistrySelect 5 (2020) 13732–13737.